J. Fluid Mech. (1980), *vol.* 100, *part* 3, *pp.* 623–638
Printed in Great Britain

An experimental and numerical study of periodic flow in a curved tube

By J. Y. LIN AND J. M. TARBELL

Department of Chemical Engineering,
The Pennsylvania State University,
University Park, Pennsylvania 16802

(Received 27 August 1979)

Fully developed periodic flow (with non-zero mean) of a Newtonian fluid in a rigid curved tube has been investigated both numerically and experimentally. Results are reported for the mean friction factor, the amplitude ratio and phase angle between flow rate and pressure drop, the axial velocity profile, and the wall shear stress distribution. The numerical results (obtained by a finite difference method) are restricted to rather slow flows (mean Dean number $\bar{D}n < 100$), while the experimental results (extracted from instantaneous flow rate-pressure drop measurements) extend up to $\bar{D}n \sim 300$. A 'resonant' interaction between the axial and secondary flows at intermediate frequencies appears to be a characteristic feature of periodic flow in a curved tube.

1. Introduction

Steady Poiseuille flow in a rigid curved tube and its effect on associated transport processes have been studied extensively since Dean (1927) first predicted the characteristic twin-vortex secondary motion (figure 1*a*) associated with this flow (see, for example, Tarbell & Samuels 1973; Kalb & Seader, 1974; Smith 1976). However, time-periodic Poiseuille flow in a rigid curved tube was first analysed only recently by Lyne (1970) who considered the problem of pure sinusoidal flow (with zero mean). Lyne constructed an asymptotic expansion solution of the Navier–Stokes equations, valid for high frequencies ($\alpha \gg 1$), and obtained a striking result. For sufficiently high frequencies ($\alpha > 12{\cdot}9$), the twin vortex motion which characterizes steady flow, transforms to a qualitatively new four-vortex motion (figure 1*b*). The inward centrifuging near the centre of the tube was indeed quite unexpected. In independent theoretical studies of this same problem, Zalosh & Nelson (1973) and Chandran *et al.* (1974), employing quite distinct solution techniques, predicted the same new four-vortex motion. These theoretical predictions of the new phenomenon were subsequently verified experimentally by Bertelsen (1975).

In this paper, we report numerical and experimental results for periodic Poiseuille flow (*with non-zero mean*) in a rigid curved tube. The only previous work on this flow was by Smith (1975) who utilized a variety of asymptotic expansions to obtain approximate solutions in the high ($\alpha \gg 1$) and low ($\alpha \ll 1$) frequency regimes. We believe that our results for intermediate frequencies reveal a significant new phenomenon – *resonance between the axial flow and the secondary flow*. This means that the

0022–1120/80/4527–2090 $02.00

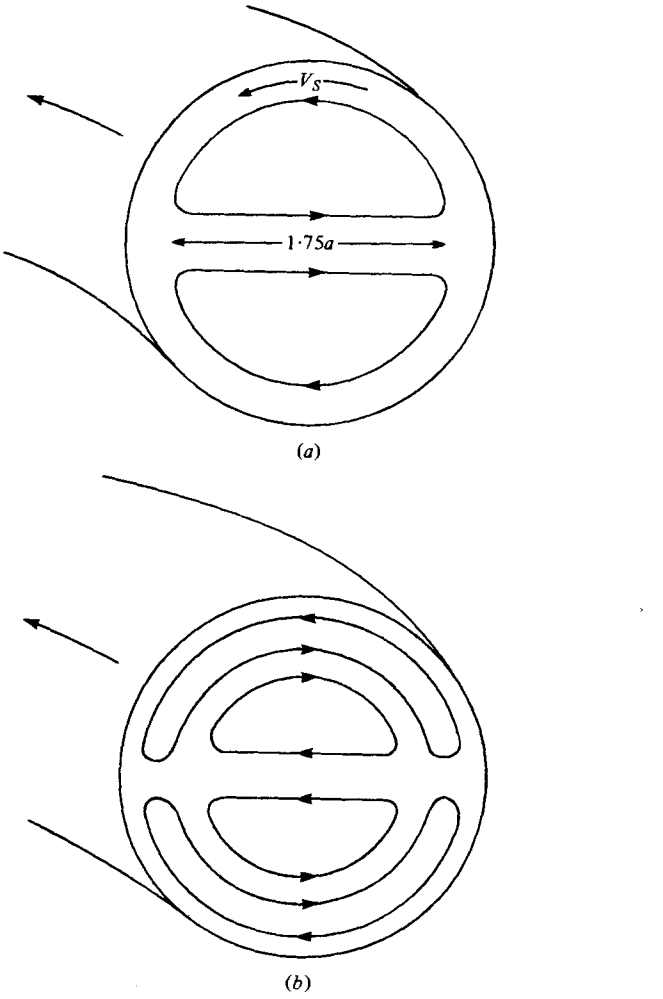

FIGURE 1. Curved tube secondary flows: (*a*) Dean-type secondary flow; (*b*) Lyne-type secondary flow.

secondary flow has a natural frequency, roughly characterized by the circulation time of the secondary flow at the time-averaged flow rate, which is excited by the oscillating axial flow over a narrow range of frequencies. The character of the resonating flow may be quite unusual and not anticipated on the basis of low frequency (quasi-steady) or high frequency (relaxed steady) information. It must be emphasized that the four-vortex secondary flow discovered by Lyne (1970) is not a manifestation of resonance since a pure sinusoidal flow contains no underlying steady motion and thus no characteristic circulation time (natural frequency).

2. Numerical methods

Solutions of the Navier–Stokes and continuity equations for fully developed laminar flow in a rigid curved tube with an imposed axial pressure gradient having the dimensionless form, $K(1+k\sin\omega t)$, were obtained by a modified 'alternating direction

implicit' algorithm. Here k is the amplitude of the oscillating pressure gradient, and ω the frequency of oscillation. The equations, the grid work and the *basic algorithm* were described by Tarbell & Samuels (1973) in connexion with the steady flow ($k = 0$) version of the problem. A detailed description of the periodic-flow algorithm is available elsewhere (Lin 1979). Briefly, in the periodic-flow algorithm, the time period $[0, 2\pi/\omega]$ was divided into N equal increments, and the *basic algorithm* was employed to integrate all fields over one period (with iteration to convergence of the stream-function–vorticity equation at every time step). During this integration, field values from the 'old' period (which unfortunately had to be stored in their entirety) were incorporated in explicit calculations whenever 'new' period values were not available. The 'new' period fields were compared with the 'old' period fields, and if adequate convergence was not apparent, additional iterations were pursued. Convergence was considered adequate when the time-averaged (denoted by a tilde) and peripherally averaged (denoted by an overbar) friction factor, $\bar{\tilde{f}}(\lambda, K, k, \alpha)$, had converged to within 10^{-4} on a relative basis.

A uniform (11×11) polar grid with 121 points covering half of the tube cross-section was employed for all periodic-flow calculations. A previous grid refinement study of the steady flow numerical solution (Tarbell & Samuels 1973) had shown that the 121 point grid could predict the peripherally averaged friction factor, $\bar{f}(\lambda, K)$, of an infinite point grid to within 0·4 % at low Dean numbers ($Dn < 12$). Grid refinement studies at higher Dean numbers were prohibited by excessive computation time. However, for Dean numbers up to 315 (the highest value computed) in a tube of aspect ratio ($\lambda \equiv R/a$, where a is the tube radius and R is the radius of curvature) 30, the $\bar{f}(\lambda, K)$ values of Tarbell & Samuels' 121 point grid calculations were within 3·0 % of those reported by Collins & Dennis (1975) who carried out more exhaustive grid refinement studies of their numerical algorithm. The Tarbell & Samuels' $\bar{f}(\lambda, K)$ values were also within 2·0 % of the experimental values reported recently by Mishra & Gupta (1979). The periodic-flow algorithm, with $k = 0$, reproduced the Tarbell & Samuels' $\bar{f}(\lambda, K)$ values exactly for all of the cases ($Dn < 43$) attempted. As a further check on the accuracy of the periodic-flow algorithm, the aspect ratio (λ) was set to 10^{10}, and attempts were made to reproduce the analytical results of Uchida (1956) for fully developed periodic flow in a straight tube. For test cases with $k = 0{\cdot}5$ and $\alpha = 6$, 9 and 16, Uchida's values for the mean friction factor were numerically computed to within 0·1 %, while his values for the amplitude ratio and phase angle were computed to within 1·0 %.

Because of the preliminary considerations described above, we have confidence in the accuracy and consistency of the numerical results to be presented. Unfortunately, our ability to obtain results with reasonable computation and storage requirements was limited by numerical stability considerations. Our experience with the algorithm indicates that the following rough stability criterion must be satisfied:

$$\alpha^2 N > 200\pi, \tag{1}$$

where N is the number of increments in one period. Since the storage limits of the IBM 370-3033 (560K bytes) were approached for $N \sim 20$, we were unable to obtain solutions for $\alpha < 5$.

The results obtained by the finite difference method are supplemented by values of the time and peripherally averaged friction factor in the low-frequency ($\alpha \to 0$)

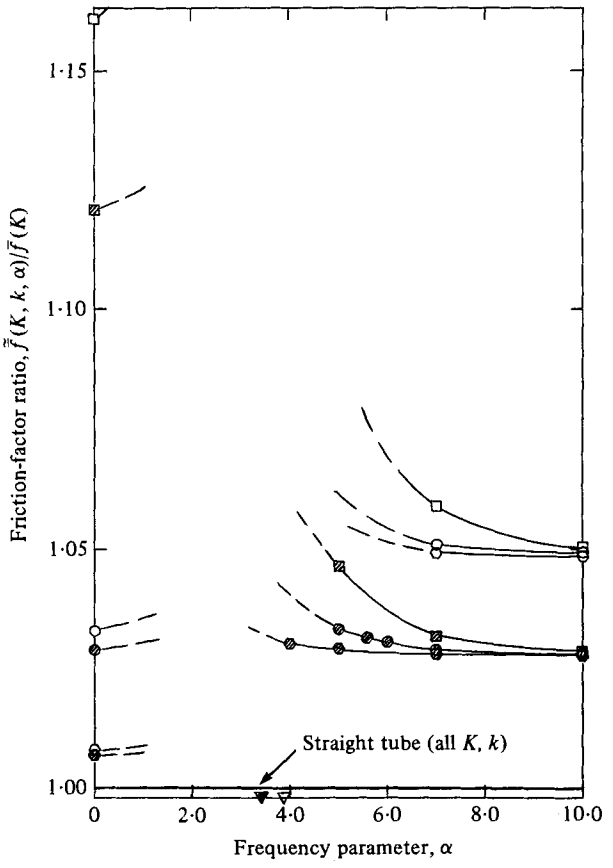

FIGURE 2. Numerical friction-factor data ($\lambda = 20$). $K = 283$: ▨, $k = 1{\cdot}0$; ⊘, $k = 0{\cdot}5$; ⊘, $k = 0{\cdot}25$; ▽, α_{res}. $K = 600$: □, $k = 1{\cdot}0$; ○, $k = 0{\cdot}5$; ○, $k = 0{\cdot}25$; ▽, α_{res}.

limit. These values are easily obtained because the periodic flow approaches a quasi-steady state as $\alpha \to 0$. This limiting low frequency friction factor

$$\bar{\tilde{f}}_0(\lambda, K, k) \equiv \lim_{\alpha \to 0} \bar{\tilde{f}}(\lambda, K, k, \alpha) \tag{2}$$

is calculated as follows:

$$\bar{\tilde{f}}_0(\lambda, K, k) = \frac{K}{\lambda \langle \tilde{w}_s \rangle^2 (\lambda, K, k)}, \tag{3}$$

where

$$\langle \tilde{w}_s \rangle (\lambda, K, k) = \frac{1}{2\pi} \int_0^{2\pi} \langle w_s \rangle (\lambda, K(1 + k \sin \tau))\, d\tau, \tag{4}$$

and $\langle w_s \rangle (\lambda, K)$ is the steady-flow, area-averaged, axial velocity which depends only on the aspect ratio (λ) and the steady pressure gradient (K). The $\langle w_s \rangle (\lambda, K)$ values of Tarbell & Samuels (1973) and a simple Simpson's rule technique were employed to evaluate the integral in equation (4).

Numerical results for the friction factor are displayed in figure 2 (additional numerical results will be discussed in § 5). The ordinate is the ratio of the time and peripherally averaged friction factor with periodic pressure gradient, $\bar{f}(K, k, \alpha)$, to the peripherally averaged friction factor under steady pressure gradient, $\bar{f}(K)$; the abscissa is the dimensionless frequency variable, α. The parameter K may be interpreted as the Reynolds number which would be obtained in a straight tube of the same

radius, and at the same pressure drop as the curved tube. The curves are not complete because of the numerical stability problem discussed previously. However, the available results suggest that there are maxima in the curves.

Evidence to support a hypothesis that maxima in the friction factor versus frequency curves are a manifestation of resonance between the axial flow and the secondary flow comes from two sources. (i) Estimates (derived below) of the characteristic circulation time of the secondary motion in curved tube flow under steady pressure gradient (K) predict the resonant frequencies (α_{res}) shown in figure 2. Clearly the maxima in the curves of friction factor versus frequency must occur at frequencies near the perdicted α_{res}. (ii) Analytical solutions of the Navier–Stokes equations for fully developed periodic flow in rigid straight tubes (Sexl 1930; Uchida 1956) predict a time-averaged friction factor which is independent of frequency and amplitude (see figure 2). This is significant because the straight-tube flow has no secondary flow – no natural frequency.

An estimate of α_{res} is developed from the definition of the resonant frequency given below:

$$\omega_{res} \equiv 2\pi \frac{V_s}{L_s}; \tag{5}$$

L_s is a characteristic path length and V_s is a characteristic path velocity for the steady secondary flow (see figure 1*a*). The following estimates are based on the work of Dravid *et al.* (1971):

$$L_S = 4{\cdot}5a; \quad V_S = \frac{\nu}{a}(0{\cdot}9656\,\tilde{D}n^{\frac{1}{2}} + 1{\cdot}65), \tag{6a, b}$$

where $\tilde{D}n$ is the time-averaged Dean number and ν is the kinematic viscosity. Equations (5) and (6) lead to the final estimate

$$\alpha_{res} = 1{\cdot}18(0{\cdot}9656\,\tilde{D}n^{\frac{1}{2}} + 1{\cdot}65)^{\frac{1}{2}}. \tag{7}$$

To verify the resonance hypothesis which was suggested by our numerical results and the estimate of equation (7), we performed a series of flow-pressure-drop experiments which are described in the next section.

3. Experimental methods

The major components of the experimental system are shown schematically in figure 3. The overall system is composed of four sections and each is described below.

Section I provides a sinusoidally varying flow rate by superimposing a sinusoidal flow oscillation on a steady flow. The steady flow is generated by a gear pump (ECO Gearchem Model G4-ACV-KKU) driven by a 0·5 hp phase motor equipped with a speed controller. The sinusoidal flow pulsations are provided by a piston pump (Harvard Apparatus Model 1423) having adjustable stroke volume (15–100 ml), stroke rate (5–100 min^{-1}) and phase ratio. The gear pump speed controller and the three piston pump controls allow adjustment of the sinusoidal pressure drop parameters (K, k, α).

Section II is a flowmeter which monitors both the instantaneous and time-averaged flow rates. It consists of a straight three-metre length of heavy wall Pyrex tube (1·27 cm inside diameter) fitted with a pair of pressure taps (0·5 cm inside diameter holes separated by 10 cm) at the far end. The pressure taps are connected to a

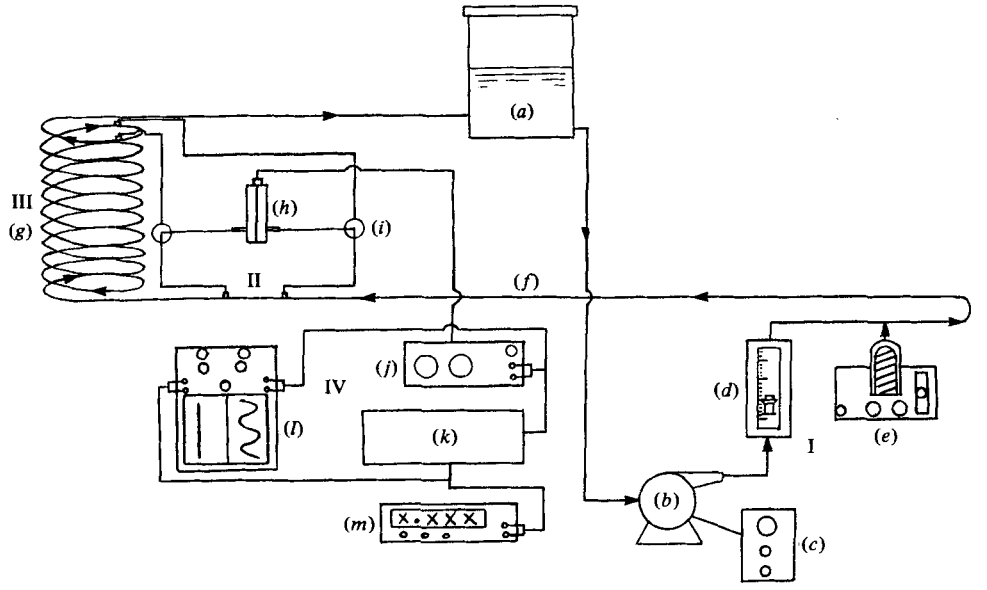

FIGURE 3. Schematic diagram of the experimental apparatus. (*a*) Constant head tank. (*b*) Gear pump. (*c*) Speed controller. (*d*) Rotameter. (*e*) Pulsatile piston pump. (*f*) Straight tube. (*g*) Helical coil. (*h*) Differential pressure transducer. (*i*) Two-way stockcock valve. (*j*) Carrier demodulator. (*k*) Low-pass filter. (*l*) Two-channel recorder. (*m*) Digital voltmeter.

differential pressure transducer (section IV) via short lengths of tygon tubing. Based on the work of Atabek & Chang (1961), the three-metre flow development length insures fully developed straight-tube periodic flow for all of our experiments. By measuring the instantaneous pressure drop for fully developed flow in the straight tube, the instantaneous flow rate may be calculated from the theory of fully developed periodic flow in straight tubes (Sexl 1930; Uchida 1956).

The operating equations of the flowmeter are quite simple as the straight tube is a linear system under fully developed flow conditions. If the measured pressure gradient has the following form:

$$\Delta P/\Delta L = K(1 + k\cos\omega t) \tag{8}$$

where P is the pressure and L the length of tube. Then the flow rate is given by

$$Q = K_q(1 + k_q\cos(\omega t - \delta)) \tag{9}$$

where K_q is the mean flow rate given by

$$K_q = \frac{K\pi a^4}{8\mu} \quad \text{Hagen–Poiseuille Law,} \tag{10}$$

and k_q is the amplitude of the flow rate,

$$k_q = \sigma k. \tag{11}$$

The parameters σ and δ are functions of the frequency parameter α ($= a(\omega/\nu)^{\frac{1}{2}}$). The functions $\sigma(\alpha)$ and $\delta(\alpha)$ may be extracted from Uchida (1956). Thus, by measuring K, k and ω, it is possible to calculate the instantaneous flow rate (K_q, k_q, δ). The flowmeter was calibrated in steady flow by a time weighing method and the Hagen–Poiseuille law was obeyed to within 0·3 % up to a Reynolds number of 1100.

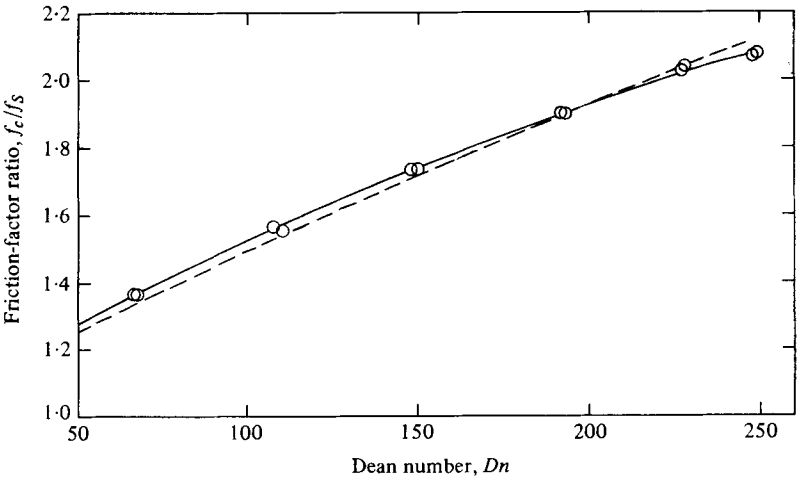

FIGURE 4. Experimental friction-factor data (steady flow, $\lambda = 15{\cdot}4$).
○, Experimental data; ——, Mishra & Gupta (1979); – – –, Tarbell & Samuels (1973).

Section III is the test section which contains a helical coil (curved tube) made from heavy wall Pyrex tube (1·15 cm inside diameter). The aspect ratio of the coil (λ) is 15·4 and the pitch is about 0·02. A pair of pressure taps (0·5 cm inside diameter holes separated by 19·3 cm) is located 194 cm downstream from the coil entrance. Based on the work of Yao & Berger (1975) and Patel, McFeeley & Jolls (1975), this entrance length ensures fully developed periodic flow in the curved tube section. Glycerol/water mixtures (2·5–4·0 cSt) provide a Newtonian test fluid.

Section IV is the data acquisition section. A differential pressure transducer (Validyne DP103, $\pm$ 0·02 psid, natural frequency $\sim$ 50 Hz) sends a.c. signals from the flowmeter and test section to a carrier demodulator (Validyne CD15) which provides a d.c. output for filtering and recording. A first-order low-pass filter (break frequency $\sim$ 0·01 Hz) is employed to time average the periodic output from the demodulator. A Gould/Brush 280 recorder (flat frequency response up to 35 Hz) displays both the instantaneous and time-averaged outputs.

4. Experimental results

A series of steady flow experiments (covering the range of time-averaged flows to be considered in subsequent periodic-flow experiments) was conducted initially. Results, in the form of the ratio of curved tube to straight tube friction factors (at the same Reynolds number) as a function of the curved tube Dean number (Dn), are compared to the theoretical results of Tarbell & Samuels (1973) and the experimental results of Mishra & Gupta (1979) in figure 4. Our experimental results are within 0·5 % of Mishra & Gupta's and this leads us to believe that the experimental system was adequately calibrated.

All of the periodic-flow experiments were characterized by a nearly pure sinusoidal flow rate and pressure gradient. Fourier analysis of several strip chart recordings indicated that the amplitude of the first harmonic was within 3·0 % of the value obtained by measuring the mean and the maximum/minimum peak height. The maxima and minima of the recordings were displaced nearly the same distance above

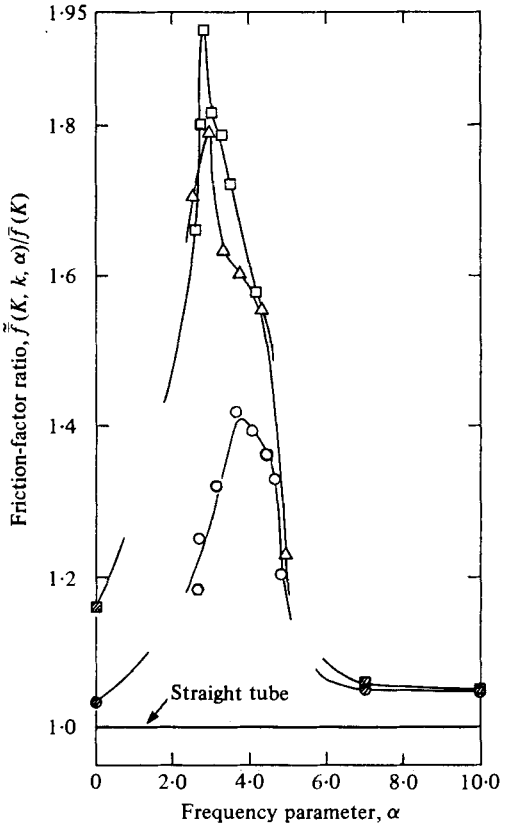

FIGURE 5. Friction factor data. Open symbols are experimental data ($K = 779$, $\lambda = 15{\cdot}4$); shaded symbols are numerical data ($K = 600$, $\lambda = 20$). □, $k = 1{\cdot}0$; △, $k = 0{\cdot}8$; ○, $k = 0{\cdot}5$.

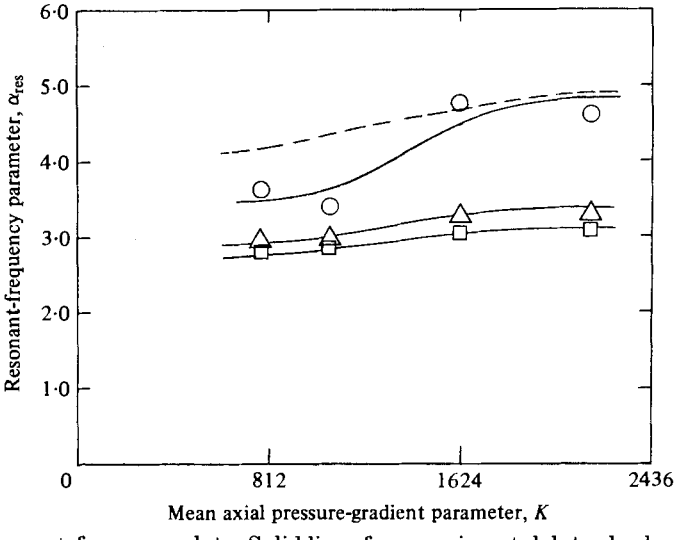

FIGURE 6. Resonant-frequency data. Solid lines for experimental data; broken line for theoretical estimate (equation (7)). □, $k = 1{\cdot}0$; △, $k = 0{\cdot}8$; ○, $k = 0{\cdot}5$.

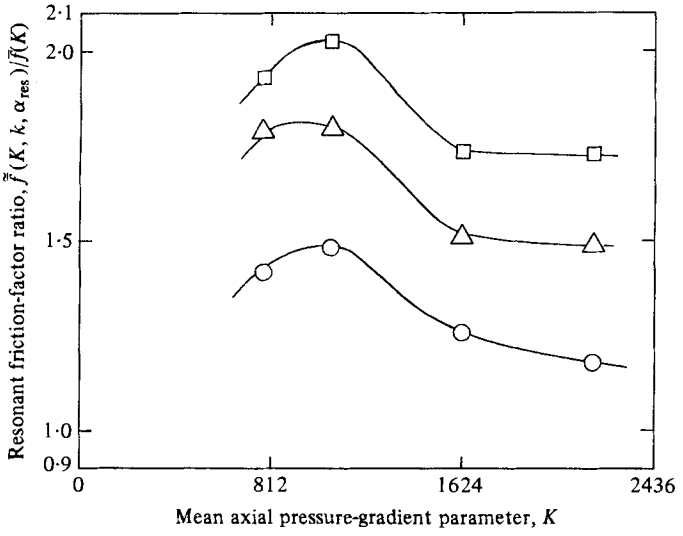

FIGURE 7. Resonant friction-factor data. □, $k = 1{\cdot}0$; △, $k = 0{\cdot}8$; ○, $k = 0{\cdot}5$.

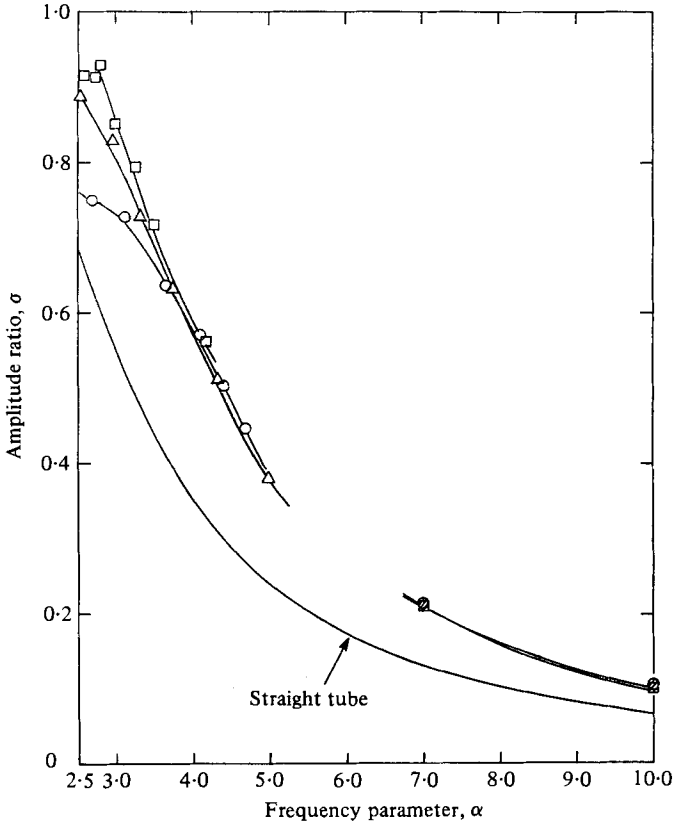

FIGURE 8. Amplitude-ratio data. Open points are experimental data ($K = 779$, $\lambda = 15{\cdot}4$); shaded points are numerical data ($K = 600$, $\lambda = 20$). □, $k = 1{\cdot}0$; ▽, $k = 0{\cdot}8$; ○, $k = 0{\cdot}5$.

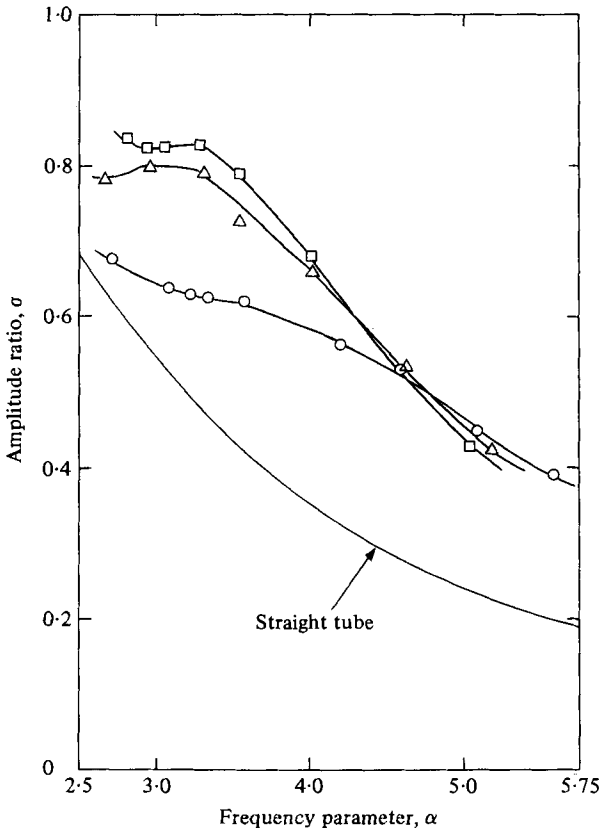

FIGURE 9. Experimental amplitude-ratio data (K = 2177, λ = 15·4). □, k = 1·0; △, k = 0·8; ○, k = 0·5.

and below the mean. Thus, even though the curved tube is a non-linear system, we have observed that a sinusoidal pressure-gradient input appears as a sinusoidal flow-rate output. This would appear to be linear behaviour. However, as we shall see, the mean and phase lag of the output, as well as the output/input amplitude ratio, depend strongly on the amplitude and mean of the input. This clearly is nonlinear behaviour.

Periodic flow experimental results were obtained at four mean pressure gradients (K = 779, 1066, 1623, 2177), three pressure-gradient amplitudes (k = 0·5, 0·8, 1·0), and several frequencies in the range $2{\cdot}5 < \alpha < 5{\cdot}5$. The mean friction factor, and the amplitude ratio and phase angle between flow rate and pressure drop were extracted from measurements of the instantaneous flow rate and pressure drop. Experiments were repeated at K = 779, k = 0·5, and K = 1623, k = 1·0 for $2{\cdot}5 < \alpha < 5{\cdot}5$. The mean friction factor, which was the most frequency-sensitive variable measured, was reproducible to within 4·0 %, while the amplitude ratio and phase angle were reproducible to within 2·0 %. Representative data are presented in figures 5–11, while a complete tabulation of all data is available elsewhere (Lin 1979).

Typical friction factor results are displayed in figure 5. The striking feature of these results is the presence of maxima at intermediate frequencies for each k. These maxima strongly support our hypothesis of resonant interaction between the axial and secondary flows. This may be seen more clearly in figure 6 which compares our

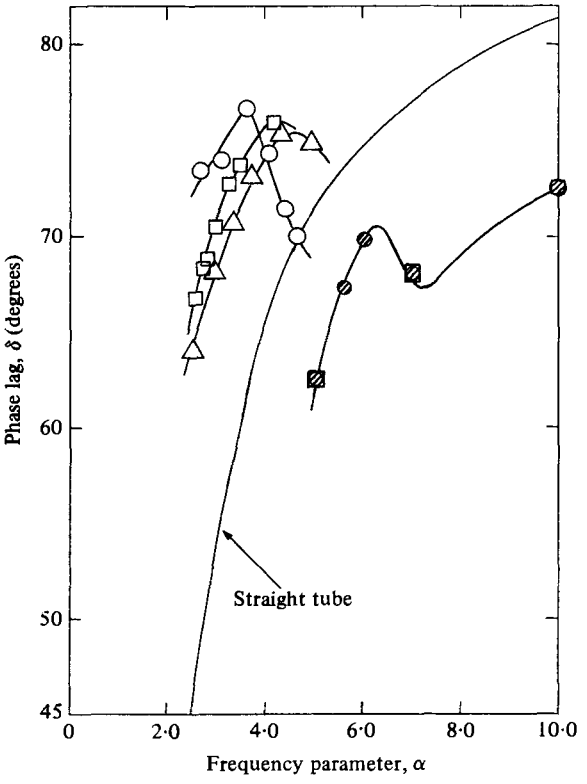

FIGURE 10. Phase-lag data. Open points are experimental data (K = 779, λ = 15·4); shaded points are numerical data (K = 283, λ = 20). □, k = 1·0; △, k = 0·8; ○, k = 0·5.

estimate of the resonant frequency (α_{res}) based on the steady secondary flow (equation (7)) with the experimentally observed resonant frequencies. If one assumes that the steady flow estimate is indicative of the low amplitude ($k \to 0$) behaviour, then the trend is clear. The resonant frequency is shifted to lower values as the driving amplitude is increased. The resonant friction factor values are also very sensitive to the amplitude (figure 7).

Figures 8 and 9 show the typical flow/pressure-gradient amplitude ratio ($\sigma = k_q/k$) dependence on frequency for the various input conditions (k, K). The amplitude ratio is always higher for the curved tube than for the straight tube. The influence of k is great at intermediate frequencies (near α_{res}) but is diminished at higher frequencies, in accord with numerical results (see figure 8). As in the case of the friction factor, the influence of K is rather weak.

The phase lag of the flow rate relative to the pressure gradient (δ) is displayed in figures 10 and 11. The experimental data indicates a maximum in the α dependence of δ for all (k, K). The limited numerical data which is included in figure 10 reveals a similar maximum which is followed by a minimum at slightly higher frequency. We may expect this minimum/maximum behaviour of the phase lag dependence on frequency to be a characteristic feature of periodic flow in a curved tube. Although not shown in figure 10, the numerical data further indicate that the phase lag approaches a high frequency asymptote ($\alpha \to \infty$) of 80·4° which is independent of K and k. This

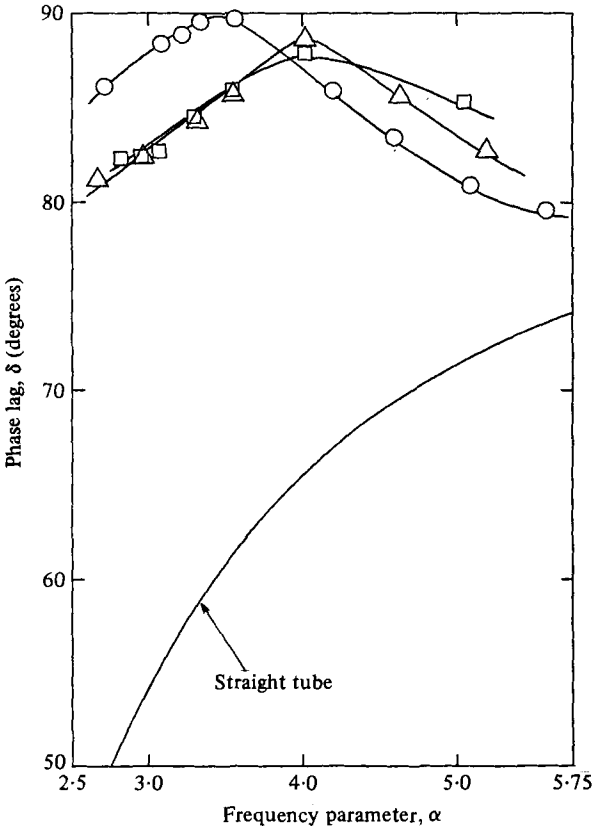

FIGURE 11. Experimental phase-lag data (K = 2177, λ = 15·4). □, k = 1·0; △, k = 0·8; ○, k = 0·5.

observation is based on limited results for $\lambda = 20$; $K = 133, 283$; $k = 0{\cdot}25, 0{\cdot}50, 1{\cdot}0$; $\alpha < 46$. It should be noted that the asymptotic ($\alpha \to \infty$) phase lag for the straight tube is always 90°. Finally, unlike the friction factor and the amplitude ratio, the phase lag displays marked dependence on K.

5. Numerical results

Flow-pressure drop data of the type presented in the last section provides a dynamic characterization of the curved tube, but is unable to shed direct light on the internal attributes of the flow field. However, the flow pressure drop data confirms our hypothesis of resonant interaction between the axial and secondary flows at intermediate frequencies. The friction-factor results suggest abnormally high wall shear stresses for resonant flows and this may have its implications for atherosclerosis – a disease whose pathogenesis is thought to be linked with local fluid mechanics and radial mass-transport rates [see the representative theories of Fry (1969) and Caro, Fitz-Gerald & Schroter (1971)]. With this in mind, we present details of the wall shear stress distribution and axial velocity profile (figures 12–14) for the case $K = 600$, $k = 1{\cdot}0$, and $\alpha = 7{\cdot}0$. This particular case provided the highest mean friction factor enhancement obtained by numerical methods (see figure 2).

The axial wall shear stress ($\tau_{r\theta}|_{y=1} \equiv -\partial w/\partial y|_{y=1}$) and the secondary wall shear

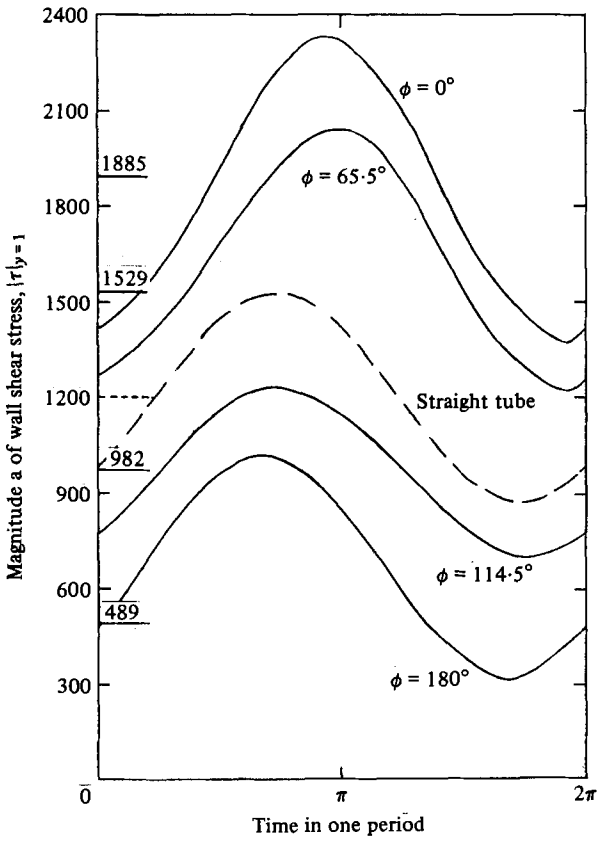

FIGURE 12. Magnitude of the wall shear stress ($K = 600$, $\lambda = 20$, $k = 1{\cdot}0$, $\alpha = 7{\cdot}0$). Solid lines for curved tube; dashed lines for straight tube; values indicated on inside of ordinate are for steady flow.

stress ($\tau_{r\phi}|_{y=1} \equiv -\partial v/\partial y|_{y=1}$) were computed from the discrete velocity fields via a three point Lagrange coefficient approximation. The magnitude of the wall shear stress ($|\tau|$) as a function of time for four peripheral locations ($\phi = 0°$ – outside wall, $\phi = 180°$ – inside wall) is shown in figure 12 together with similar results for periodic flow in a straight tube (from Uchida 1956) and steady flow in a curved tube (from Mori & Nakayama 1965).

The variation in wall shear stress is perhaps the most striking feature of these results. Consider the ratio of maximum to minimum wall shear stress taking into account both temporal and spatial variations. The following values are obtained:

Steady flow, straight tube,	$\lvert\tau\rvert_{\max}/\lvert\tau\rvert_{\min} = 1{\cdot}00$;
Periodic flow, straight tube,	$\lvert\tau\rvert_{\max}/\lvert\tau\rvert_{\min} = 1{\cdot}75$;
Steady flow, curved tube,	$\lvert\tau\rvert_{\max}/\lvert\tau\rvert_{\min} = 3{\cdot}85$;
Periodic flow, curved tube,	$\lvert\tau\rvert_{\max}/\lvert\tau\rvert_{\min} = 7{\cdot}40$.

Apparently the outside wall experiences unusually high shear stress and the inside wall experiences unusually low shear stress during periodic flow in a curved tube. This trend may be amplified at lower frequencies near the resonant frequency.

The periodic axial velocity profile (horizontal plane) for the curved and straight

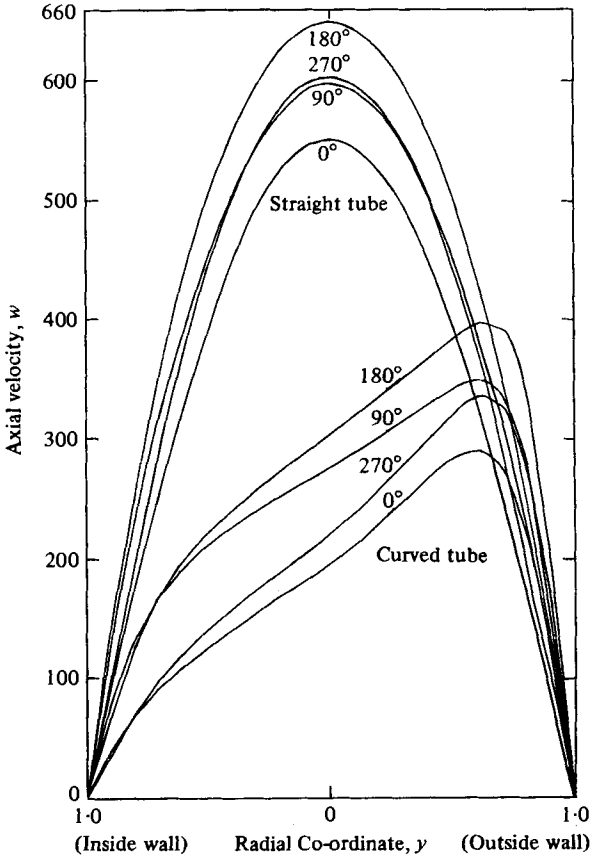

FIGURE 13. Axial velocity profile in the horizontal plane ($K = 600$, $\lambda = 20$, $k = 1{\cdot}0$; $\alpha = 7{\cdot}0$).

tubes are displayed in figure 13. The reduced flow and skewed velocity profile in the curved tube are very apparent and qualitatively similar to steady flow curved tube behaviour. Figure 14 shows the pulsatile component of the axial velocity profile obtained by subtracting the mean values from those in figure 13. Unlike the straight-tube profile, the curved-tube profile is quite asymmetric about the centre-line. It should be noted that for pure pulsatile flow (zero mean) in a curved tube, the axial velocity profile is quite symmetric (Zalosh & Nelson 1973), again in contrast with the behaviour found here. All of the numerical solutions displayed instantaneous secondary flows of the twin vortex Dean type (figure 1*a*). No four-vortex Lyne type (figure 1*b*) secondary flows were observed. However, resonant frequencies were not reached by numerical methods, and thus the nature of the resonant secondary flow remains unknown.

6. Concluding remarks

The interaction between the axial and secondary fluid motion during periodic flow in a curved tube leads to flow behaviour which is markedly frequency dependent at intermediate frequencies. We have termed this phenomenon 'resonance' because the

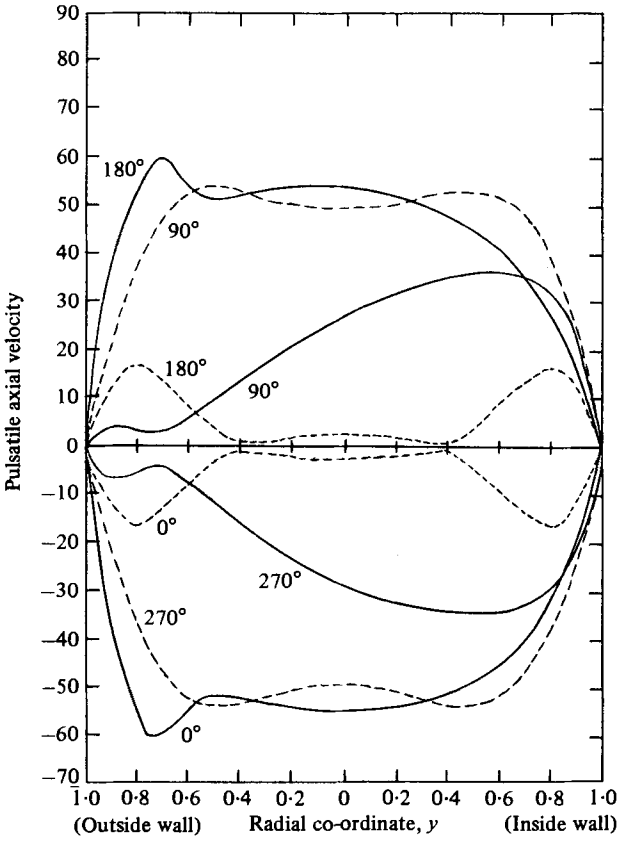

FIGURE 14. Pulsatile component of the axial velocity in the horizontal plane ($K = 600$, $\lambda = 20$, $k = 1{\cdot}0$, $\alpha = 7{\cdot}0$). ——, curved tube; – – – –, straight tube.

sensitive frequency range appears to be centred about the natural circulation frequency of the secondary motion. The time and peripherally averaged axial shear stress at the wall (or equivalently, the friction factor) is relatively much higher in the narrow resonance region than at high or low frequencies. One may expect similar enhancement of radial heat and mass transfer rates at frequencies near the resonant frequency. One should also expect resonance phenomena to occur more generally in 'periodic Poiseuille flows with secondary motion'.

Resonance may play a role in the pathogenesis of atherosclerosis. This seems plausible because of the pattern of the disease. It occurs in the large arteries (where the blood flow is highly pulsatile) and preferentially in regions of curvature and branching (Nerem & Cornhill 1978). Both curvature and branching induce secondary flows which can interact with the axial flow in a resonant fashion such as we have reported here. The resonance may affect the wall shear stresses and mass transport rates – quantities generally thought to be important in the disease mechanism (Fry 1969; Caro *et al.* 1971).

Partial support for this work by NSF Grant ENG 77-06083 is gratefully acknowledged.

REFERENCES

ATABEK, A. B. & CHANG, C. C. 1961 *Z. angew. Math. Phys.* **12**, 185.

BERTELSEN, A. F. 1975 *J. Fluid Mech.* **70**, 519.

CARO, C. G., FITZ-GERALD, J. M. & SCHROTER, R. C. 1971 *Proc. Roy. Soc.* B **177**, 109.

CHANDRAN, K. B., SWANSON, W. M., GHISTA, D. N. & VAYO, H. W. 1974 *Ann. Biomed. Engng* **2**, 392.

COLLINS, W. M. & DENNIS, S. C. R. 1975 *Quart. J. Mech. Appl. Math.* **28** (2), 133.

DEAN, W. R. 1927 *Phil. Mag.* **4**, 208.

DRAVID, A. N., SMITH, K. A., MERRILL, E. W. & BRIAN, P. L. T. 1971 *A.I.Ch.E. J.* **17** (5), 1114.

FRY, D. L. 1969 *Circ. Res.* **24**, 93.

KALB, C. E. & SEADER, J. D. 1974 *A.I.Ch.E. J.* **20** (2), 340.

LIN, J. Y. 1979 Periodic Flow in a Curved Tube. Ph.D. thesis, Dept. of Chem. Engng, Pennsylvania State University.

LYNE, W. H. 1970 *J. Fluid Mech.* **45**, 13.

MISHRA, P. & GUPTA, S. N. 1979 *Ind. Engng Chem. Process Des. Dev.* **18**, 130.

MORI, Y. & NAKAYAMA, W. 1965 *Int. J. Heat Mass Transfer* **8**, 67.

NEREM, R. M. & CORNHILL, J. F. 1978 The Role of Fluid Mechanics in Atherogenesis. *Proc. from a Specialists Meeting, Columbus, Ohio.*

PATEL, R. D., MCFEELEY, J. J. & JOLLS, K. R. 1975 *A.I.Ch.E. J.* **21**, 259.

SEXL, TH. 1930 *Z. Phys.* **61**, 349.

SMITH, F. T. 1975 *J. Fluid Mech.* **71**, 15.

SMITH, F. T. 1976 *Proc. Roy. Soc.* A **347**, 345.

TARBELL, J. M. & SAMUELS, M. R. 1973 *Chem. Engng J.* **5**, 117.

UCHIDA, S. 1956 *Z. angew. Math. Phys.* **7**, 403.

WOMERSLEY, J. R. 1955 *J. Physiol.* **127**, 553.

YAO, L. S. & BERGER, S. A. 1975 *J. Fluid Mech.* **67**, 177.

ZALOSH, R. G. & NELSON, W. G. 1973 *J. Fluid Mech.* **59**, 693.